X-ray emission of a xenon gas jet plasma diagnosed with Thomson scattering

C. Chenais-Popovics, V. Malka, and J.-C. Gauthier
Laboratoire pour l'Utilisation des Lasers Intenses, École Polytechnique, 91128 Palaiseau, France

S. Gary, O. Peyrusse, and M. Rabec-Le Gloahec
Commissariat à l'Énergie Atomique, Boîte Postale 12, 91680 Bruyères-le-Châtel, France

I. Matsushima
National Institute of Advanced Industrial Science and Technology, Tsukuba 3058568, Japan

C. Bauche-Arnoult, A. Bachelier, and J. Bauche
Laboratoire Aimé Cotton, Bâtiment 505, Campus d'Orsay, 91405 Orsay, France
(Received 22 June 2001; revised manuscript received 28 November 2001; published 10 April 2002)

We present the results of a benchmark experiment aimed at validating recent calculation techniques for the emission properties of medium and high-Z multicharged ions in hot plasmas. We use space- and time-resolved M-shell x-ray spectroscopy of a laser-produced gas jet xenon plasma as a primary diagnostic of the ionization balance dynamics. We perform measurements of the electron temperature, electron density, and average charge state by recording simultaneous spectra of ion acoustic and electron plasma wave Thomson scattering. A comparison of the experimental x-ray spectra with calculations performed *ab initio* with a non-local-thermodynamic-equilibrium collisional-radiative model based on the superconfiguration formalism, using the measured plasma parameters, is presented and discussed.

DOI: 10.1103/PhysRevE.65.046418 PACS number(s): 52.50.Jm, 52.25.Os, 32.70.Fw, 52.70.La

I. INTRODUCTION

The capability to accurately predict multicharged ion radiative properties in plasmas not in local thermodynamic equilibrium (NLTE) is of primary interest because such conditions are ubiquitous in laboratory and astrophysical plasma studies [1]. Indeed, NLTE plasmas are found in inertial confinement fusion (ICF) [2], tokamaks [3], z-pinch plasmas [4], coherent x-ray sources [5], and ultra-short pulse laser-produced plasmas [6], to name a few. Most of these plasmas are made of medium- and high-atomic number elements for which little spectroscopic data is known apart from the isoelectronic sequences of helium, neon, and nickel. The simple line structure of bound-bound transitions prevails only for low-Z plasmas. As the number of bound electrons become large, the lines become so close to each other that they cannot be resolved and the number of ions taking part in plasma emission increases. Accordingly, the development of NLTE atomic physics calculations for heavy elements is a challenge for the understanding of emission and absorption x-ray spectra from which the ionic composition and the average charge $\langle Z \rangle$ of the plasma can be deduced. This is a particularly important parameter in ICF plasma studies because the value of $\langle Z \rangle$ determines laser absorption, electron heat conduction, collision rates, acoustic velocities, and the radiation energy balance.

Calculation of complete spectra of high-Z elements in plasmas by detailed atomic structure codes and level population models incorporating several ions would need an unmanageable number of transitions and energy levels. Despite this difficulty, we have to tackle this problem because spectral formation is an invaluable tool for providing information on the plasma parameters by looking directly at the emission spectrum, using spectroscopy as a noninterfering plasma probe. Statistical emission calculation methods based on unresolved transition arrays (UTA) [7], in which transitions are bunched in transition arrays and super transition arrays (STA) [8], have been developed for interpreting unresolved spectral patterns for systems in LTE. These methods have been extended, very recently, to NLTE situations [9,10]. Ionic populations in NLTE plasmas are calculated with a collisional radiative model, which requires collisional and radiative transition rates between all energy levels of all ionic stages. In Ref. [11], the most recent developments in atomic physics applicable to complex spectra are presented showing clearly the step-by-step evolution from the UTA to the STA approaches and from LTE to NLTE situations.

Accordingly, it is important to provide a method in which NLTE calculations can be benchmarked against well-characterized experimental data. In an attempt to reach this goal, very recent experiments in laser-irradiated argon gas bags [12], in laser-produced plasmas on gold targets [13,14], and in inertial confinement fusion *Hohlraums* [15] have been performed. We present here a detailed comparison of theoretical x-ray spectra to experimental data obtained in a laser-heated xenon gas jet plasma, in which the electronic temperature, the electron density, and the average charge state $\langle Z \rangle$ are measured from electronic and ionic Thomson scattering spectra. We used a gas jet plasma source because it provides homogeneous and adjustable ionic densities. Gas jets have been used previously for investigating the complex M shell spectroscopy of xenon [16–18], but without any characterization of the plasma state. Calculations, performed with the measured plasma parameters, using the AVERROES/TRANSPEC NLTE collisional-radiative superconfiguration code [10], and also with an ion-by-ion spin-orbit-split arrays (SOSA) approach [19] are compared to experiments.

II. EXPERIMENTAL SYSTEM

The measurements were performed in a xenon ($Z=54$) laser-heated sonic gas jet. From a 1 mm diameter nozzle, a parabolic atomic density profile was obtained, fully characterized by He-Ne laser interferometry [20]. The atomic density was found nearly constant (within 8%) over the central 400 μm diameter of the jet. The atomic density varied linearly with pressure in the investigated range of 1.2–11 bar. A frequency-doubled ($\lambda=526.6$ nm) laser beam of the Nd:glass nanosecond Laboratoire pour l'Utilisation des Lasers Intenses facility was focused at the center of the gas jet with an $f/2.5$ lens equipped with a random phase plate, providing a 160 μm full width at half maximum focal spot diameter. The laser pulse had a flat top shape with a 650 ps duration and 100 ps rise time. When the pressure was below 5 bar, the laser energy was absorbed along the whole jet dimension, and the x-ray emitting plasma was filling the jet diameter along the laser axis. Most of the data presented here have been obtained with a pressure of 4.2 bar. The corresponding ion density is 4.75×10^{18} cm^{-3} on the jet axis, at a distance of 1 mm from the nozzle. An $f/3$ lens was set at 45° from the heating beam to collect the Thomson scattering (TS) signal. The collection volume (200 μm long, 100 $\times100$ μm wide) was located inside the laser-heated volume as shown in Fig. 1(a). Time-resolved ionic Thomson spectral features were obtained by imaging the scattered radiation dispersed by a 1200 lines/mm grating spectrometer onto the entrance slit of a visible streak camera with 200 ps/mm sweep speed. The measured spectral resolution was 0.25 Å. The temporal resolution was limited by the spectrometer (≈50 ps) because of the variation of the optical path length with wavelength. Time-resolved electronic TS spectra were measured using a lower dispersion spectrometer (100 lines/mm) giving a spectral resolution of about 100 Å. In this case, the streak camera (30 ps time resolution) was used with a 100 ps/mm sweep speed. The resulting time-resolved spectra were recorded on a 12 bit charge-coupled device (CCD) camera. Calibration of the ion density in between the xenon shots was performed by recording TS spectra of a helium gas jet plasma. Indeed, the neutral density depends only on the adiabatic parameter γ which is the same for all monoatomic gases ($\gamma=5/3$), and the electron density measurement of fully ionized helium plasmas ($\langle Z\rangle=2$) provides the ion density.

Both time-integrated and time-resolved x-ray spectrographs were equipped with a thallium-hydrogen-phthalate crystal and set at 90° from the laser axis [see Fig. 1(b)]. Spectral resolution was around 50 mÅ, limited by the laser focal spot diameter. The time-integrated x-ray spectra were resolved in space with a 250 μm slit perpendicular to the laser axis. Time-integrated spectra were recorded on Kodak DEF films and corrected for crystal [21], filters, and film [22] responses. Alignment of the laser beams and the gas jet was checked with visible and x-ray imaging CCD cameras. From the spatial measurement of the neutral density and the space-resolved, time-integrated x-ray images, we found that the gas jet geometry allows us to obtain a plasma volume of 400 μm length and about 200 μm diameter where the ion density and the electron temperature are fairly homogeneous.

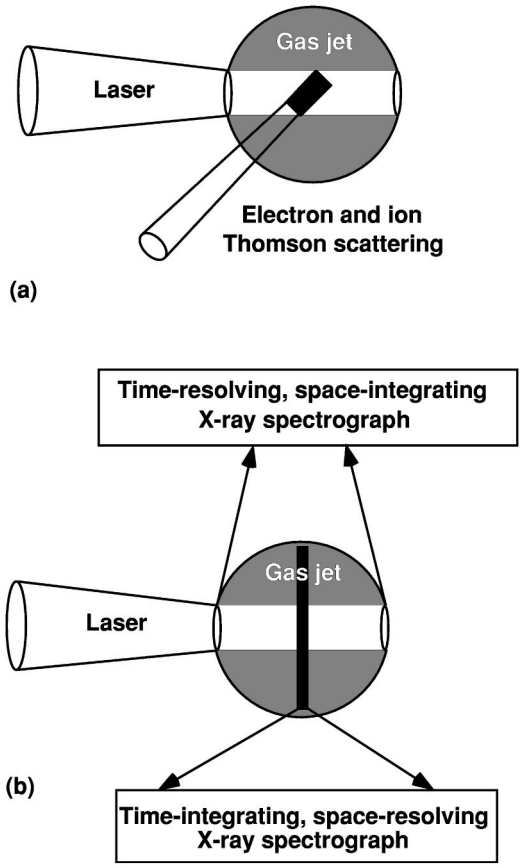

FIG. 1. Geometry of the experiment. The Thomson scattering diagnostic observation volume (a) and the x-ray spectrograph line of sights (b) are shown together with the diameter of the gas jet and the laser-heated region.

For the x-ray spectroscopic diagnostic, the integrating volume along the line of sight of the spectrograph covers the homogeneous ion density laser-heated region, and a layer of cold xenon which has been taken into account in the analysis (see Fig. 1).

III. RESULTS AND DISCUSSION

A typical ionic Thomson scattering image is shown in Fig. 2. A strip has been extracted (see arrow in Fig. 2) and compared to theory [23]. After an ionization phase (around 200 ps) in which the ionic satellite spectral positions vary rapidly and their width is broadened by the extended ion charge distribution, steady ionic features appear clearly during the laser-pulse duration. The electronic components of the spectra (not shown here) are shifted on both sides of the fundamental frequency. The electronic density is deduced from the position of the electronic satellites. A small decrease of their shift during the laser pulse denotes a very slow reduction of the density due to plasma expansion. Then, the average charge $\langle Z\rangle$ is deduced from the ratio of the measured electron and ion densities. As the electron-ion thermalization time is larger than the laser pulse for the density achieved

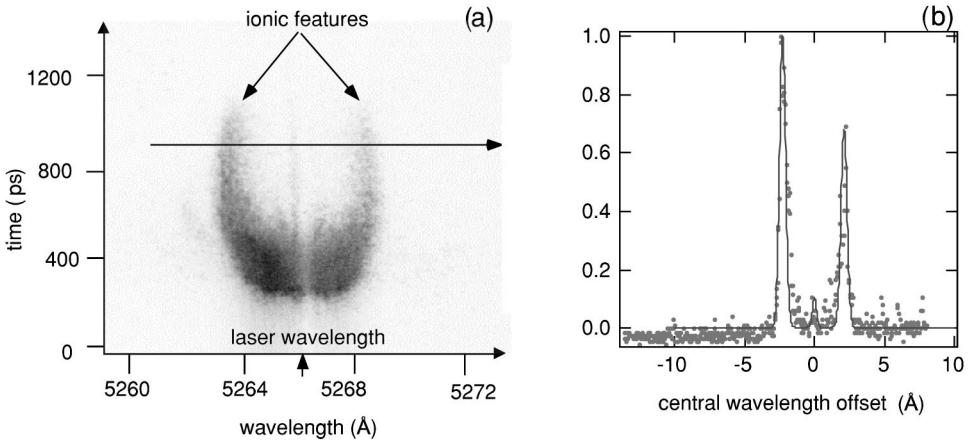

FIG. 2. (a) Typical ionic Thomson scattering spectrum as a function of time. A strip of attenuating material has been positioned on the detector to hide the strong electron feature signal around the laser wavelength at 5266 Å. (b) Strip (dots) taken at the position indicated by the horizontal arrow superimposed on the theoretical fit (solid line). Time origin is arbitrary. The laser pulse has a 650 ps flat top with 100 ps rise time.

here, we assume that $T_e \gg T_i$. The electron temperature is then determined from the frequency separation of the two peaks of the TS ion feature which is twice the ion acoustic frequency [24,25]. The parameters determined by fitting simultaneously the electron and ion TS spectra (see Fig. 2) measured at the laser maximum, for a pressure of 4.2 bar, are: $T_e = 415 \pm 40$ eV, $\langle Z \rangle = 27.4 \pm 1.5$, $n_e = 1.30 \pm 0.05 \times 10^{20}$ cm^{-3}. This gives a scattering parameter $\alpha = 3.43$, well into the collective regime of TS.

Figure 3 shows the time-resolved M-shell xenon spectrum obtained in the 11 Å wavelength range for a pressure of 4.2 bar. In this specific laser shot, a second laser pulse was sent in the plasma 1 ns after the onset of the main pulse. The emission was studied as a function of time for each of the two laser pulses. The spectral shape of the x-ray emission remains the same for the duration of the first laser pulse. This is representative of the other results presented in this paper, which were obtained using only one laser pulse. The same behavior has been seen in time-resolved spectra measured in the 13 and 14 Å spectral ranges. This strongly suggests that the ion density and the ionization balance that determine the line intensity and the line ratios, respectively, are unchanged during the laser pulse. This is consistent with the TS diagnostic results that are also unchanged during most of the laser pulse. The x-ray time-resolved spectra, therefore, demonstrate that the time-integrated, space-resolved measurements that cover a wider spectral range can be interpreted with confidence by assuming that the plasma parameters vary only slightly over the duration of the laser pulse.

Time-integrated x-ray spectra measured at the center of the gas jet for a gas pressure of 4.2 bar and a single laser pulse are presented in Fig. 4. The $3d$-$4f$ transition arrays appear at wavelengths larger than 12.5 Å. Different ion species have been identified around the closed-shell Ni-like Xe^{26+} ion, i.e. Xe^{25+} (Cu-like) to Xe^{29+} (Mn-like). The Xe^{27+} Co-like and Xe^{28+} Fe-like ions are the dominant fea-

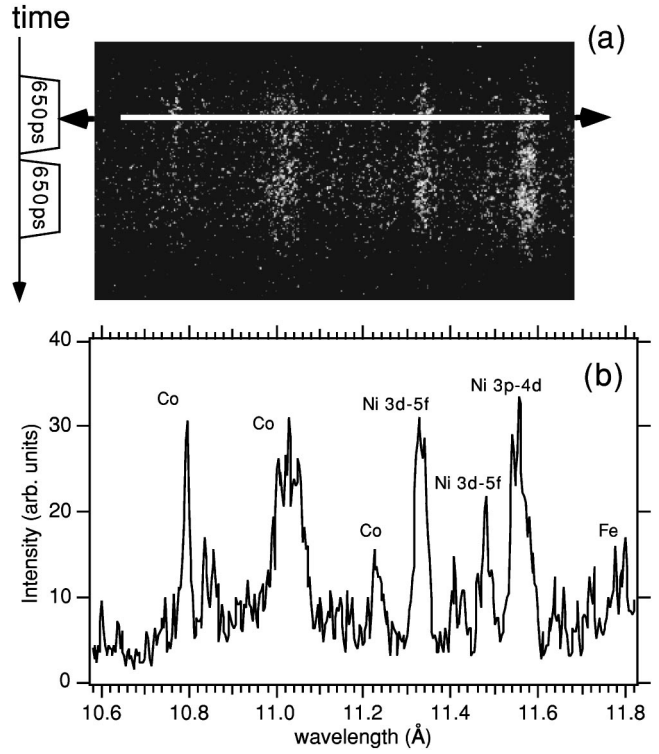

FIG. 3. (a) Time-resolved x-ray spectrum obtained in the 11 Å range for a xenon pressure of 4.2 bar. (b) Strip (horizontal arrow) with the ion labeling of the spectral features. The laser pulse shapes are given on the left of the top image.

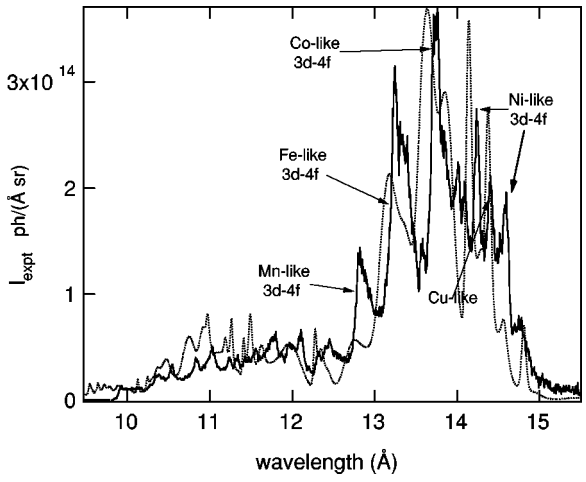

FIG. 4. Time-integrated experimental spectrum (solid line) compared to the AVERROES/TRANSPEC calculation (dotted line) for $T_e = 450$ eV, $n_i = 4.75 \times 10^{18}$ cm^{-3}.

tures. Nickel-like $3d$-$4f$ transitions at 14.23 Å (from the $4f_{5/2}$ jj-coupled spin orbital) and 14.63 Å (from the $4f_{7/2}$ jj-coupled spin orbital) are prominent. In addition, different Xe^{26+} and Xe^{27+} spectral features have been identified in the 9.5–12.5 Å range which covers mainly the $3p$-$4d$, $3d$-$5f$, and $3d$-$6f$ transitions. In the wavelength range 10.6–11.8 Å, the time-integrated spectrum of Fig. 4 displays the same spectral features as the time-resolved spectrum shown in Fig. 3. Small differences in the line ratios and the underlying continuum slope can be explained by the fact that the observation volume is not the same in the two configurations (see Fig. 1) and that the time-resolved data was not corrected for the streak camera response.

The synthetic x-ray spectrum shown in Fig. 4 has been calculated *ab initio* with plasma conditions determined from the TS diagnostic. Collisional and radiative rates were generated with the AVERROES calculations based on the superconfiguration and supertransition array (STA) concepts. These data were then used in the population kinetics model TRANSPEC which calculates the x-ray spectra, for a given electron temperature and density. This calculation can also be used as the postprocessor of a hydrodynamic code [26].

The result of the calculation performed with AVERROES/TRANSPEC and the parameters taken from the TS diagnostic, i.e., $T_e = 415$ eV and $n_i = 4.75\ 10^{18}$ cm^{-3} gives an average charge $\langle Z \rangle$ slightly too low to reproduce the experimental ratios between the different $3d$-$4f$ structures in the range 13–15 Å. The agreement is better when we increase the temperature to 450 eV, the upper limit of the estimated error bar in TS measurements. In these calculations, reabsorption was introduced with a 160 μm length, and the spectral resolution was fixed at the instrumental value of 50 mÅ. The comparison between the experiment and the model around 13 Å shows that the Fe-like Xe^{28+} and the Mn-like Xe^{29+} ions are underpopulated, taking the Co-like Xe^{27+} ion as a reference. The two intense calculated peaks between 14 and 14.5 Å, which could be attributed at first sight to Ni-like Xe^{26+} $3d$-$4f$ features, have to be interpreted carefully. First, the intensity of these peaks is exaggerated because Ni-like features are merged in the calculation with Cu-like features. Second, the Ni-like features are calculated with an atomic potential which is not accurate enough (see the discussion below) to reproduce Ni-like transition wavelengths [27]. We note that a global shift of the theory of about $+90$ mÅ would give a much better quantitative agreement for the wavelength positions of the different ion spectral features. Finally, the intensity ratio between the $3d$-$4f$ features around 14 Å and the $3d$-$5f$/$3d$-$6f$ features around 11 Å is correctly reproduced.

To explain the remaining discrepancies between theory and experiment seen in Fig. 4, it is important to discuss some aspects of the *ab initio* AVERROES/TRANSPEC NLTE calculations. The present spectrum calculations were performed with the same set of superconfigurations as the one used for computing NLTE populations. To be more specific, no subsequent splitting of the superconfigurations was invoked after the convergence on $\langle Z \rangle$ was obtained. As a consequence, the spectrum is fully consistent with the excitation/ionization kinetics. This detail is important because the STA method is known to show different convergence properties on the ionic populations and on the spectrum itself [11]. This last remark holds both for LTE and NLTE situations. In the present calculation, consistent refinement of the spectrum is still feasible but it would involve a large and prohibitive number of superconfigurations. An alternative would be to use the effective temperature concept to deal with the departure from LTE within the superconfigurations [28]. This powerful method which should also reduce the number of superconfigurations necessary for the kinetics calculations is still under development. Another source of discrepancy is the configuration interaction problem which is difficult to handle in the superconfiguration approach, except when one treats the breakdown of jj coupling in a manner similar to the one developed in the spin-orbit-split array (SOSA) method [29]. Such a problem is visible in Fig. 4, particularly on the calculated $3d$-$4f$ Co-like peaks around 13.74 Å which should coalesce into a single peak with a long-wavelength shoulder, as in the experiment. This discrepancy underlines some possible improvements in our treatment of the configuration interaction effect between SOSA arrays. Finally, we stress that such modeling performed *ab initio* with measured plasma parameters is very recent, to our knowledge, and still in a development stage [30].

TABLE I. Ion fractions obtained with the SOSA fit and with the AVERROES/TRANSPEC code. The average charge is respectively $\langle Z \rangle = 26.5$ for the SOSA calculation and $\langle Z \rangle = 26.8$ for AVERROES.

Isoelectronic sequence	Zn-like	Cu-like	Ni-like	Co-like	Fe-like	Mn-like
Ion charge	24	25	26	27	28	29
SOSA fit	0.010	0.030	0.595	0.249	0.096	0.021
AVERROES	0.065	0.080	0.312	0.365	0.188	0.044

Another approach to the modeling of complex spectra is to use the SOSA method for each individual ion, adjusting the ion population with a least-squares-fit procedure. This method has proved to be useful in the analysis of radiatively heated nickel absorption spectra [31]. In the present case, the resulting spectrum is globally very similar to what is calculated with the AVERROES/TRANSPEC code. Apart from the ion distribution itself, the only other parameter for the fit is the temperature used for calculating the configuration population distribution relevant to each ion; we have taken a value of 400 eV consistent with TS measurements. Table I gives the ion distribution obtained from this fit, compared to the distribution found with the *ab initio* AVERROES/TRANSPEC calculation. The ion distributions and the average charge given by the two codes are close—$\langle Z \rangle = 26.5$ and 26.8— in agreement with the TS measurement. An LTE calculation would give a much higher $\langle Z \rangle$, around 40, and thus a very different spectrum.

IV. CONCLUSION

In conclusion, we have recorded stationary space-resolved experimental x-ray spectra of xenon that we have reproduced

with *ab initio* calculations using the plasma parameters provided by simultaneous electronic and ionic Thomson scattering diagnostics. Both time-resolved Thomson scattering spectra and time-resolved spectroscopic data show that the central region of the plasma jet is stationary during the laser pulse. We have shown that a laser-heated gas jet, in which plasma parameters are fully determined by Thomson scattering independently from the x-ray spectra, is an interesting benchmark for NLTE atomic physics codes. Our experimental results may be considered as a test bed for the improvement of these codes.

Of course, the STA approach, because of its compactness, does not provide the spectroscopic quality that could reproduce quantitatively the position of the spectral features. However, we have now at our disposal a good framework for emission calculations of medium- and high-*Z* plasmas, which will play an important role in laboratory plasma studies with large lasers, such as the National Ignition Facility or the Laser Megajoule inertial confinement fusion projects. This model should also play a role in the design of plasma-based x-ray sources for applications. The next step of this work would be to combine the AVERROES/TRANSPEC codes to a radiative hydrodynamic simulation of the experiment [26].

ACKNOWLEDGMENTS

We would like to thank Jean-François Wyart for helpful discussions and identification of several xenon x-ray lines. We are indebted to Franck Gilleron for his help in the data analysis. The support of the technical staff of LULI, in particular, Raymond Konig, was particularly appreciated. LULI is ''Unité Mixte de Recherche No. 7605, CNRS-CEA-Université Paris VI–École Polytechnique.''

[1] R.W. Lee *et al.*, Lawrence Livermore National Laboratory, Report No. UCRL-ID-119170, 1995 (unpublished).
[2] J.D. Lindl, Phys. Plasmas **2**, 3933 (1995).
[3] K.B. Fournier, D. Pacella, M.J. May, M. Finkenthal, and W.H. Goldstein, Nucl. Fusion **37**, 825 (1997); K. Asmussen, K.B. Fournier, J.M. Laming, R. Neu, J.F. Seely, R. Dux, W. Engelhardt, and J.C. Fuchs, *ibid.* **38**, 967 (1998).
[4] K.G. Whitney *et al.*, Rev. Sci. Instrum. **8**, 3708 (2001).
[5] *X-ray Lasers 2000*, 7th International Conference on X-ray Lasers, edited by G. Jamelot, C. Möller, and A. Klisnick (EDP Sciences, Les Ulis, 2001).
[6] P. Gibbon and E. Förster, Plasma Phys. Controlled Fusion **38**, 769 (1996), and references therein.
[7] J. Bauche and C. Bauche-Arnoult, in *Laser Interactions with Atoms, Solids and Plasmas*, edited by R.M. More (Plenum Press, New York, 1994).
[8] A. BarShalom, J. Oreg, W.H. Goldstein, D. Shvarts, and A. Zigler, Phys. Rev. A **40**, 3183 (1989).
[9] A. Bar-Shalom, J. Oreg, and M. Klapisch, Phys. Rev. E **56**, R70 (1997).
[10] O. Peyrusse, J. Phys. B **33**, 4303 (2000).
[11] M. Klapisch, A. Bar Shalom, J. Oreg, and D. Colombant, Phys. Plasmas **8**, 1817 (2001).
[12] S. Glenzer *et al.*, Phys. Rev. E **62**, 2728 (2000).
[13] S. Glenzer *et al.*, Phys. Rev. Lett. **82**, 97 (1999); M. Foord *et al.*, *ibid.* **85**, 992 (2000).
[14] Bo Bai, Jian Zheng, Wandong Liu, C.X. Yu, Xiaohua Jiang, Xiaodong Yuan, Wenhong Li, and Z.J. Zheng, Phys. Plasmas **8**, 4144 (2001).
[15] S. Glenzer *et al.*, Phys. Rev. Lett. **87**, 045002 (2001).
[16] H. Fiedorowicz *et al.*, Appl. Phys. B: Lasers Opt. **70**, 305 (2000).
[17] S. Doron *et al.*, Phys. Rev. A **59**, 188 (1999).
[18] I.Yu. Skobelev *et al.*, J. Phys. B **32**, 113 (1999).
[19] C. Bauche-Arnoult, J. Bauche, and M. Klapisch, Phys. Rev. A **31**, 2248 (1985); J. Bauche, C. Bauche-Arnoult, and M. Klapisch, J. Phys. B **24**, 1 (1991).
[20] V. Malka *et al.*, Rev. Sci. Instrum. **71**, 2329 (2000).
[21] A. Burek, Space Sci. Instrum. **2**, 53 (1976).
[22] B.L. Henke *et al.*, J. Opt. Soc. Am. B **3**, 1540 (1986).
[23] J. Sheffield, *Plasma Scattering of Electromagnetic Radiation* (Academic, New York, 1975), p. 130.
[24] S. Glenzer *et al.*, Phys. Plasmas **6**, 2117 (1999).
[25] V. Malka *et al.*, Phys. Plasmas **8**, 2605 (2001).
[26] O. Peyrusse, J. Quant. Spectrosc. Radiat. Transf. **71**, 571 (2001).
[27] J.-F. Wyart (private communication).
[28] C. Bauche-Arnoult and J. Bauche, J. Quant. Spectrosc. Radiat. Transf. **71**, 189 (2001).
[29] J. Bauche, C. Bauche-Arnoult, and M. Klapisch, J. Phys. B **24**, 1 (1991).
[30] A. Bar-Shalom, J. Oreg, and M. Klapisch, J. Quant. Spectrosc. Radiat. Transf. **65**, 43 (2000).
[31] C. Chenais-Popovics *et al.*, Phys. Rev. E **65**, 016413 (2001).